R. L. HULSTROM*
Martin Marietta Aerospace
Denver, Colorado 80201

The Cloud Bright Spot

Clouds can cause an increase in solar radiation that can affect a remote-sensing technique which utilizes reflected energy.

INTRODUCTION

EVERYONE familiar with remote sensing, whether simple photography or a complex multispectral scanner, is aware of the common influences of clouds. These more common influences are, of course, shadows and/or complete obscuration of ground targets. The following sections present some field measurements and analyses that show a third cloud effect resulting in increased, as compared to nominal *clear* conditions, solar radiation incident at the ground. In addition to these measurements, Hanson[1] (1960) reported measuring "anomalous total global radiation" on an Antarctic snowfield that exceeded the extraterrestrial radiation (solar constant) for over an hour. For simplicity, this phenomenon will be referred to as *cloud bright spots* as opposed to cloud shadows.

ABSTRACT: *A cloud effect, called "cloud bright spot," is presented in terms of field measurements, theory, and significance to remote sensing. Field measurements of global solar radiation show that clouds can cause ground "bright spots" having a 30 percent higher incident solar radiation flux than surrounding areas. The possible cause and recommendations concerning ground truth measurements and instrumentation are also presented.*

One important aspect of a bright spot, in addition to having abnormally high values of incident solar radiation, is that an interpreter of the remote sensor data probably cannot readily identify such bright spots as compared to the more obvious shadows. For example, such bright spots might be interpreted as areas of high surface reflectance. The following discussion also addresses the significance of bright spots to various remote sensing techniques. Recommendations are made for simple field monitoring instrumentation to be used during remote sensing missions such as the NASA ERAP, ERTS, and EREP programs.

BASIC CONCEPTS CONCERNING GLOBAL SOLAR RADIATION

The measurements presented in the following sections are of global solar radiation, defined as the downward direct and diffuse solar radiation as received on a horizontal surface from a solid angle of 2π. The appropriate equation for this relationship is:

$$K\downarrow(\Delta\lambda) = S(\Delta\lambda) + D(\Delta\lambda) \qquad (1)$$

where K is the global solar radiation, S is the vertical component of direct solar radiation, D is the sky radiation (diffuse solar radiation), and $\Delta\lambda$ represents some increment of wavelength λ. The vertical component of the direct solar radiation is that radiation coming from the solid angle of the sun's disc, as received on a horizontal surface. It is expressed as

$$S(\Delta\lambda) = I(\Delta\lambda) \cos\theta_0 \qquad (2)$$

where I is the solar radiation coming from the solid angle of the sun's disc on a surface perpendicular to the axis of the solid angle, and θ_0 is the solar zenith angle. These quantities and relationships are illustrated in Figure 1.

The direct solar beam $I(\Delta\lambda)$ can further be

* This research was partly supported by subcontract to the Colorado School of Mines under NASA Grant NGL 06-001-015, The Bonanza Remote Sensing Project.

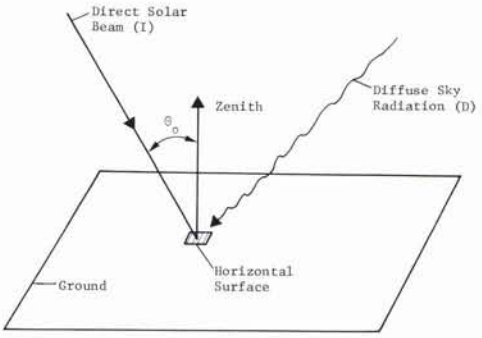

FIG. 1. Illustration of global solar radiation, sky radiation, and direct solar radiation.

represented in terms of atmospheric effects (attenuation) by

$$I(\Delta\lambda) = (R^2/R_m{}^2) I_0(\Delta\lambda)\, e^{-\tau(\Delta\lambda) \sec \theta_0} \quad (3)$$

where $I_0(\Delta\lambda)$ is the solar radiation on a surface perpendicular to the solar beam outside the Earth's atmosphere when the Earth is at its mean distance R_m from the sun (solar constant), *sec* θ_0 represents the optical path length through the atmosphere; R is the sun-Earth distance at the time of measurement of $I(\Delta\lambda)$. $R^2/R_m{}^2$ is commonly referred to as the reduction factor for mean sun-Earth distance. The expression $\tau(\Delta\lambda)$ is commonly referred to as the extinction coefficient which is composed of the molecular scattering (Rayleigh) extinction coefficient $\tau_R(\Delta\lambda)$, the aerosol scattering extinction coefficient $\tau_S(\Delta\lambda)$, and the absorption extinction coefficient $\tau_A(\Delta\lambda)$; thus,

$$\tau(\Delta\lambda) = \tau_R(\Delta\lambda) + \tau_S(\Delta\lambda) + \tau_A(\Delta\lambda). \quad (4)$$

In this paper, only a qualitative description of these extinction coefficients is needed, which is:

$$\tau_R \propto 1/\lambda^4 \qquad \text{(Rayleigh's theory)}$$
$$\tau_S \propto 1/\lambda^\alpha$$

when $0 < \alpha^\circ < 4$ (Mie scattering). The expression $\tau_A(\Delta\lambda)$ is highly selective depending on wavelength, i.e., $\tau_A(\Delta\lambda)$ is high if λ corresponds to an absorption band of water vapor, ozone, oxygen, etc.

The sky radiation D is composed of diffuse, scattered solar radiation from the molecular atmosphere (Rayleigh scattering) $D_R(\Delta\lambda)$, the diffuse, scattered solar radiation from atmospheric aerosols (Mie scattering) $D_S(\Delta\lambda)$, and solar radiation reflected from and/or transmitted by clouds $D_C(\Delta\lambda)$; thus,

$$D(\Delta\lambda) = D_R(\Delta\lambda) + D_S(\Delta\lambda) + D_C(\Delta\lambda). \quad (5)$$

As $\tau_R(\Delta\lambda)$ is inversely proportional to wavelength to the fourth power, much more molecular scattering of solar radiation occurs in the shorter wavelengths. This is readily apparent to the human eye on clear days; the sky radiation appears blue in color. As the sky becomes hazy, the sky radiation may become white/gray in color, indicating that the degree of scattering is more uniform with respect to wavelength, i.e., $\tau_S(\Delta\lambda)$ and $D_S(\Delta\lambda) \approx 1/\lambda^{1.3}$. However, if the aerosols have a small radius (on the order of the wavelength of the incident solar radiation) they can scatter in a *bluish* manner. The spectral distribution of $D_C(\Delta\lambda)$ is of a *white* nature, as is readily apparent upon observing normal clouds.

The global solar radiation can now* be given in more detail as

$$K\downarrow(\Delta\lambda) = I_0(\Delta\lambda) \cos\theta_0\, e^{-(\tau_R + \tau_S + \tau_A) \sec \theta_0} + D_R(\Delta\lambda) + D_S(\Delta\lambda) + D_C(\Delta\lambda). \quad (6)$$

With this equation the following measurements can be interpreted and analyzed.

INSTRUMENTATION AND MEASUREMENTS

The following measurements of global and sky radiation were made with two Eppley Model 2 spectral pyranometers (Figure 2). The Eppley instruments have calibration constants of 5.03 and 5.20 millivolts (mv) per cal. cm.$^{-2}$ min.$^{-1}$.

The instruments were set up at the Waterton Test Site (Figure 3), located approximately 18 miles southwest of Denver, Colo. The site elevation is approximately 6,200 feet above sea level; its coordinates are 105.13° longitude and 39.50° latitude. An insignificant influence from the Rocky

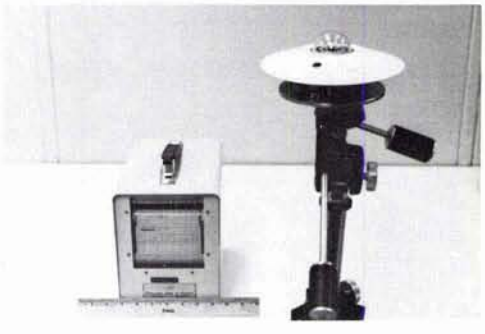

FIG. 2. Eppley Model 2 pyranometer and ICA Model 400 recorder used to measure global solar radiation.

* According to Ångstrom[2] (1930), and Volz[3] (1956), $\alpha = 1.3$ is a reasonable value.

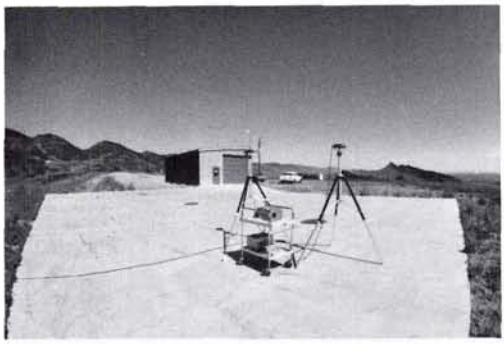

FIG. 3. Waterton Test Site and solar radiation measuring instrumentation.

Mountains front range exists with respect to global and sky radiation. This is because one of the mountains substends a solar elevation angle of greater than 5° (see IGY Instruction Manual, Part VI); actually it substends 7°. The corresponding azimuth angle substended is only 7°, making any influence even less likely.

The outputs of the Eppleys were recorded on two ICA Model 400 recorders. This combination results in an accuracy of 0.010 cal. cm.$^{-2}$ min.$^{-1}$, a sensitivity of 0.005 cal. cm.$^{-2}$ min.$^{-1}$ and a three-second, full-scale response time.

The resultant measurements shown in Figures 4 and 5 were obtained by equipping one Eppley (5.20 mv calibration constant) with a WG-7 filter, transparent from 0.295 to 2.80 micrometers (μm) and the other Eppley with an RG-8 filter transparent from 0.700 to 2.80 μm. This combination resulted in measurements of global solar radiation from 0.295 to 0.700 μm (by deduction), 0.295 to 2.80 μm, and 0.700 to 2.80 μm. The type of cloud that caused the global radiation environment shown in Figures 4 and 5 was documented with a fisheye photograph (Figure 6).

The measurement shown in Figure 7 is simply global radiation in the 0.295 to 2.80 μm region, but it represents the effects of a different cloud type (Figures 8 and 9) than the one shown in Figure 6.

The measurements shown in Figure 10 were made by continuously shading one Eppley while allowing the other to measure global solar radiation. This resulted in a simultaneous record of the effects of a cloud on the diffuse sky radiation, D (0.295 to 2.80 μm), and the global radiation $K\downarrow$ (0.295 to 2.80 μm).

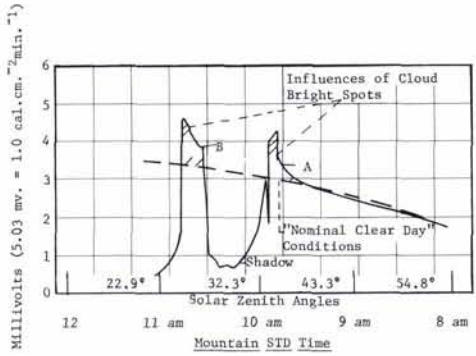

FIG. 5. Global solar radiation in the 0.700–2.8 μm region.

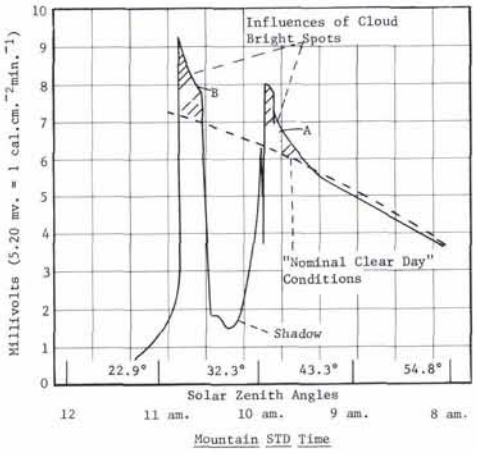

FIG. 4. Global solar radiation in the 0.295–2.80 μm region.

FIG. 6. Fisheye photograph of cloud that caused bright spots shown in Figures 4 and 5.

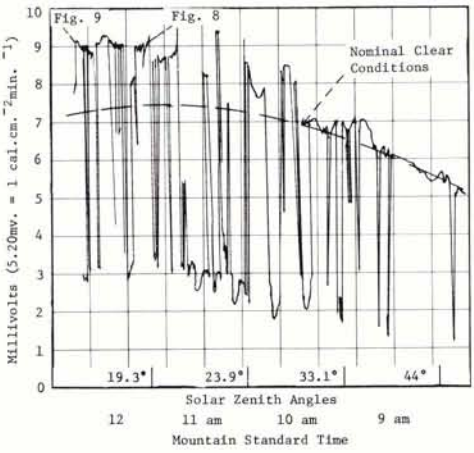

FIG. 7. Global solar radiation showing effects of clouds in the 0.295–2.8 μm region.

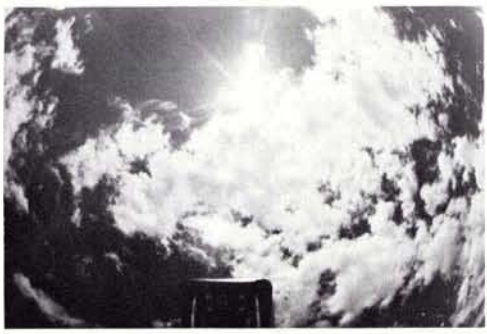

FIG. 8. Fisheye photograph of cloud that caused bright spots shown in Figure 7.

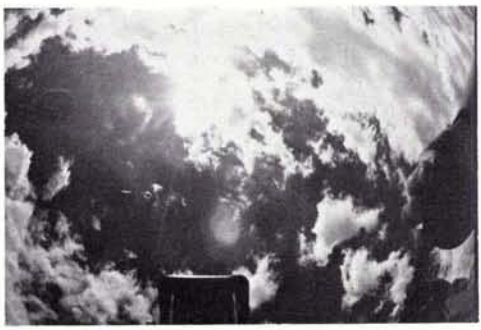

FIG. 9. Same cloud shown in Figure 8, slightly later in time.

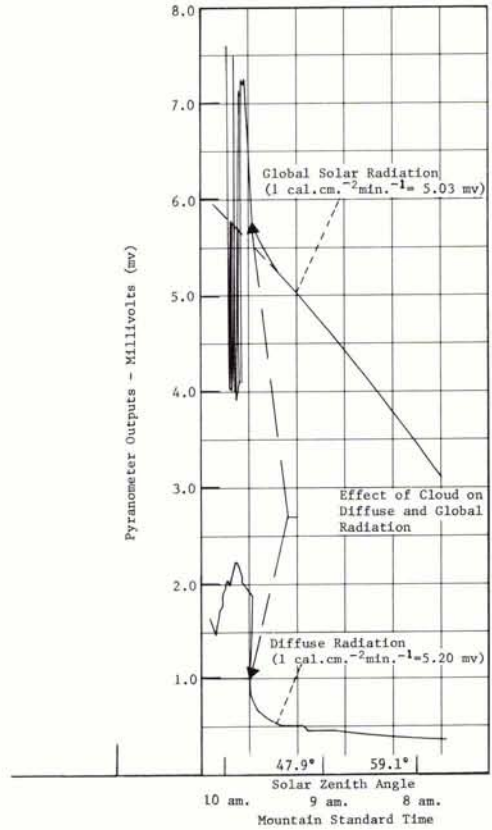

FIG. 10. Simultaneous recordings of global and diffuse radiation.

INTERPRETATION AND ANALYSIS OF MEASUREMENTS

All of the measurements shown in Figures 4,5,7, and 10 are given in terms of millivolts of sensor output as plotted against zenith angle θ_0. To obtain absolute units of cal. cm.$^{-2}$ min.$^{-1}$, simply multiply the sensor output by the reciprocal of the specific sensor's calibration constant. Each set of measurements (except those in Figure 10) are referenced to a specific cloud type and cover by use of a fisheye photograph (Figures 6,8,9).

For each set of measurements a *nominal clear day* curve is given for comparison with the cloud effects. For Figures 4, 5, and 10, this *clear* day curve was generated by computer extrapolation of the actual measured *clear* day conditions that existed prior to the onset of cloud influences. Such an extrapolation is possible by performing measurements during the *clear* conditions in order to derive the atmospheric extinction coeffi-

cient (given in Equation 6), and the ratio of sky radiation to global radiation. Knowing these two parameters, and by calculating θ_0 for various times of day, an extrapolation can be made for the remainder of the day based on actual measurements during the "clear" conditions by using Equation 6. For Figure 7, conditions were never "clear" and therefore the extrapolation method could not be used. Instead, nominal values characteristic of the test site for τ, and the ratio of sky to global radiation were picked and then used to compute the extrapolation.

The results shown in Figures 4 and 5 indicate that the cloud bright spot shown in Region *A* has about a 27-percent increase over *clear* conditions in the 0.295 and 2.80 μm region, and a 26.5-percent increase in the infrared, 0.700 to 2.80 μm region. The cloud bright spot shown in Region *B* has a 23-percent increase in the 0.295 to 2.80 μm region and a 24-percent increase in the infrared region. The fact that the percentage increases caused by the cloud are about equal for both wavelength regions is not surprising because clouds are known to scatter and/or reflect in a *white* manner.

The results shown in Figure 7 indicate much more sporadic cloud bright spots which were caused by the nature of the clouds and their rapid movement across the sky as compared to the cloud shown in Figure 6, which had a very slow movement across the sky. The percentage increases caused by the cloud shown in Figures 8 and 9, vary widely but do cause increases as high as 21 percent.

Measurements in Figure 10 show simultaneous records of the sky radiation $D(\Delta\lambda)$ and the global radiation $K\downarrow(\Delta\lambda)$ for the 0.295 to 2.80 μm region. The results indicate a 0.28 cal. cm.$^{-2}$ min.$^{-1}$ increase (20 percent) in the global solar radiation due to the cloud bright spots, and a 0.28-cal. increase (290 percent) in the sky radiation. Hence the increase in global radiation is equal to the increase in sky radiation. The magnitude of the global radiation during a bright spot is then attributed to the already existing direct solar beam, the normal sky radiation, plus the cloud radiation. The 290-percent increase in sky radiation attributed to $D(\Delta\lambda)$ then accounts for the 20-percent increase in global radiation.

In order to describe fully the physical situation that results in a cloud bright spot, one would have to conduct much more detailed measurements than those reported here. The major unknowns that should be measured are the exact geometrical relationships between the direct solar beam, the cloud(s), the ground-based sensor, and the nature of the cloud(s) in terms of height, thickness, etc. From measurements of all these variables one could perhaps determine what set of conditions result in the occurrence of cloud bright spots.

One candidate explanation of the cloud bright spot is the reflection of the direct solar beam off the cloud and onto the ground (Figure 11).

Salomonson[4] (1968) performed aircraft measurements of cloud reflectance and concluded that "clouds and snow at large solar zenith angles exhibited pronounced reflection going away from the sun and stratus clouds also exhibited a lesser increase in reflection back toward the sun."

With respect to a bright spot, the reflection is not off the cloud top, but off the edge of the cloud. Thus, as shown in Figure 11, it is likely that, at large solar zenith angles with respect to the cloud's edge zenith, strong reflections occur toward the ground. The magnitude of the reflected radiation would also be a function of the cloud edge surface area. With much more detailed measurements, as mentioned above, the cloud-bright-spot phenomenon could be compared to the reflectance measurements off the cloud tops as reported by Salomonson. However this would be difficult because the edges of clouds tend to change rapidly both in orientation (zenith) and size.

The cloud shown in Figure 6 seems to be a case in point of the reflection phenomenon. It is shown that the sun, cloud, and sensor are in the geometrical relationship illustrated in Figure 11. The bright spots labeled as *A* and *B* in Figures 4 and 5, are caused by reflection off the leading edge of the cloud. In between *A* and *B* a deep shadow exists. If

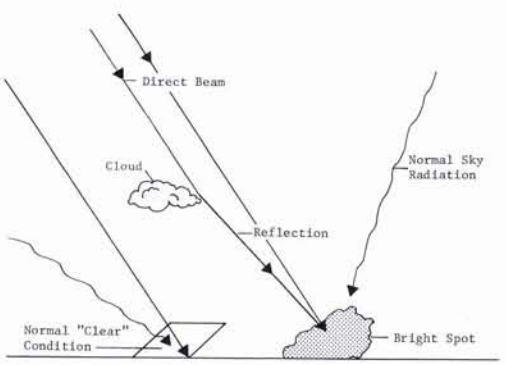

FIG. 11. Cloud reflection causing a bright spot on the ground.

one then considers very heterogenous clouds moving across the sky, the sporadic bright spots shown in Figure 7 might be explained. The bright spot shown in Figure 10 may have been caused by a very sharp reflection off the cloud which rapidly moved into the exact conditions needed for reflection. Again, it should be pointed out that much more detailed measurements are needed to define the physical and geometrical relationships that cause bright spots.

Significance of Cloud Bright Spots to Remote Sensing

Cloud bright spots can affect any remote-sensing technique that, in some manner, records the reflected solar energy (*signature*) off a ground target. This results from the fact that targets under the influence of a cloud bright spot have an incident solar radiation flux that is abnormally greater than the surrounding areas; therefore the contrast that exists between the target and its normal surroundings is not the natural contrast. In addition, if the target's reflected radiance is actually being measured, the measurement will be in error. As shown herein, this error could be as much as 30 percent. The influence of a cloud bright spot on an aircraft and spacecraft remote sensor is shown in Figure 12.

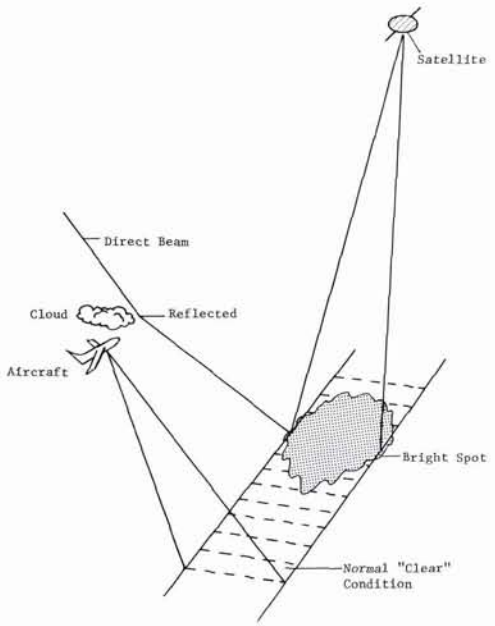

FIG. 12. Cloud-bright-spot effect on aircraft and satellite remote sensing.

The cloud-bright-spot effect on a multispectral line scanner image and photography would be a false contrast recorded in the scan and the photograph. However, with widely varying contrasts that already exist in natural scenes, the cloud bright spot would probably go undetected.

If a cloud bright spot was detected and measured on the ground during a multispectral scanner overflight, corrections to the scanner data could possibly be made by operating on the data with a correction factor derived from the ground measurements. This factor would simply be the ratio of the normal *clear* conditions to the incident global radiation measures in the bright spot area. By applying this factor to each of the scanner channel data, the bright spot data could be normalized to the *clear* conditions. If spectral measurements of the incident radiation are taken in the normal *clear* areas, similar spectral measurements would not be necessary for the cloud bright spot area because the incident radiation is increased fairly uniformly with respect to wavelength.

Such scanner data corrections are extremely difficult to apply because of the wide ground coverage normally performed in remote-sensing missions, especially satellite remote sensing. To use the corrections, one would need extensive ground measurements of the global solar radiation over the entire ground track. The minimal correction/attention given to cloud bright spots with respect to scanner imagery and photography is that the interpreter should be aware of the fact that if any shadows exist in the imagery, there is likely to be cloud bright spots as well.

Figure 12 shows a narrow field-of-view satellite remote sensor measuring the reflected radiance off a ground target under the influence of a cloud bright spot. The resulting data would be in error as much as 30 percent. The narrow-field-of-view remote sensor is particularly susceptible to cloud bright spots because the area of coverage of both is similar. Although the exact coverage area of bright spots has not been determined, they most certainly are on the order of a fraction of a kilometer or greater.

The Skylab EREP S191 Infrared Spectrometer can be seriously affected by cloud bright spots as it has a 0.46-km ground coverage. Because of its narrow field of view and pointability, it is intended to be used to collect target radiance even if broken clouds exist in the target area. Under such conditions, cloud bright spots would likely be present. However, due to the fact that the

S191 is pointed at a known target, suitable measurements of the global solar radiation would easily be made that would quantitatively describe the error and could be used to normalize the S191 data.

Recommendations for Bright Spot Ground Truth Measurements

As mentioned previously, it would be extremely difficult to instrument completely a remote sensing site in order to detect and evaluate the cloud bright spot influences. This is true for sensors which cover large ground areas such as a scanner and conventional photography. However, a continuous recording of the test site global radiation environment on position at the site would indicate whether the particular clouds passing over that position actually caused bright spots. This would, in addition to calibrating the incident global solar radiation environment, give an indication of the probability of other areas of the site being similarly influenced by the same cloud type.

If one uses a narrow field-of-view remote sensor on a specific area less than a kilometer in size, it is almost imperative to measure continuously the incident global solar radiation if any broken clouds were in the vicinity. As mentioned previously, the Skylab EREP S191 operates with this limited field. Therefore it is recommended that, despite the particular discipline (geology, agriculture, etc.) involved, candidate S191 test sites employ measurements of the global solar radiation.

Instrumentation for Cloud Bright Spot Ground-Truth Measurements

Instrumentation for measuring the effects of clouds on global solar radiation and recording this data, do not have to be complex. All that is required is a pyranometer (180° field-of-view) and a suitable strip chart recorder. An example of such a combination is shown in Figure 13. It is important to use a fast response (about 3 sec full-scale) instrument and recorder because of the rapid fluctuations in global solar radiation that can result from cloud bright spots and shadows; an example of this is shown in Figure 10. Also a strip chart record during clear conditions will directly indicate to the observer/interpreter the nature of the global solar radiation conditions during the normal *clear* state. The interpreter, using this reference, can readily determine if any abnormalities were caused by clouds in the vicinity.

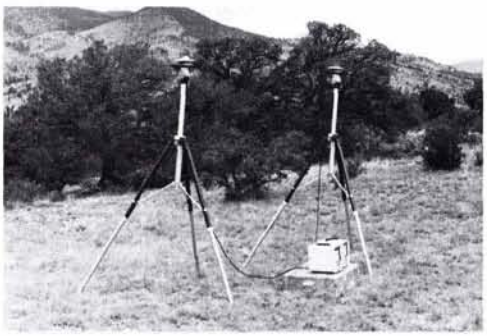

FIG. 13. Typical field setup of global solar radiation monitoring instrumentation on the Bonanza test site (NASA Site No. 185, ERAP Mission No. 168).

Acknowledgement

The author wishes to express his appreciation to Dr. A. J. Drummond and Mr. H. W. Greer of the Eppley Laboratories for their recommendations concerning instrumentation.

References

1. Hanson, K. J.: "Radiation Measurement on the Antarctic Snowfield, a Preliminary Report," *Journal of Geophysical Research*, Vol. 65, No. 3, pp. 935–945, 1960.
2. Ångstrom, K.: "On the Atmospheric Transmission of Sun Radiation, II," *Geogr. Ann. 12*, 131, 1930.
3. Volz, F.: "Optik des Dunstes," *Handb. Geophys. 8*, Kap. 14, 1956.
4. Salomonson, V.: "Anistropy in Reflected Solar Radiation," Contract NASr-147, Colorado State University, Atmospheric Sciences Paper No. 128, 1968.